Journal of Volcanology and Geothermal Research 278–279 (2014) 14–24

Contents lists available at ScienceDirect

Journal of Volcanology and Geothermal Research

journal homepage: www.elsevier.com/locate/jvolgeores

Saltation threshold for pyroclasts at various bedslopes: Wind tunnel measurements

Guilhem Amin Douillet [a,*], Keld R. Rasmussen [b], Ulrich Kueppers [a], Deborah Lo Castro [c], Jon P. Merrison [d], Jacob J. Iversen [d], Donald B. Dingwell [a]

[a] Earth & Environmental Sciences, Ludwig Maximilian University, Munich, Germany
[b] Institute of Geocience, University of Aarhus, Denmark
[c] Istituto Nazionale di Geofisica e Vulcanologia, Sezione di Catania, Italy
[d] Institute of Physics and Astronomy, University of Aarhus, Denmark

ARTICLE INFO

Article history:
Received 2 August 2013
Accepted 27 March 2014
Available online 12 April 2014

Keywords:
Pyroclasts
Wind tunnel
Saltation threshold
Surface roughness

ABSTRACT

Pyroclastic density currents represent one of the most destructive hazards associated with explosive volcanism. This destructive nature does not only urge the need for but also prevents the obtainment of in situ measurements of their physical characteristics. The resulting deposits offer, however, evidence of the physics of their sedimentation phase. Deposits of dilute pyroclastic density currents frequently exhibit repeated cycles of deposition and erosion, yielding insights into the turbulent shearing along the ground. The utilization of such field observations can be greatly enhanced by the calibration of physical properties of such flows under well-constrained laboratory conditions. Here, wind tunnel measurements were performed using pyroclastic particles. The saltation threshold and surface roughness length were calculated for wind above a pyroclastic bed. The results serve as an aid in linking field observations to quantitative values of turbulent shear at the base of a flow. Scoria and pumice particles were investigated as a function of grain size (1 ϕ fractions between 0.125 and 4 mm), as well as the influence of bedslope (−20° to +25° in 10° steps). The results point to the dominant control of density, grain size and, contrary to previous assumptions, differ moderately from results obtained for round beads. Properly utilized, the dataset enables the establishment of a link between the grain size of natural deposits and the shearing extant during their emplacement. Depending on the type of sedimentary structure observed in the field, the saltation threshold can be used as a minimal or a maximal shearing limit during emplacement of dilute pyroclastic density current deposits. Stoss-aggrading laminations likely involve the saltation threshold as an upper limit, whereas for truncation events it must have been overcome. The effect of particle concentration within the flow, a critical parameter for pyroclastic density currents and the extent of validity of the data, are discussed.

1. Introduction

1.1. Particle transport

When a fluid flowing over an erodible bed reaches a certain speed profile, known as the fluid threshold, loose particles on the bed begin to move. Erosion, transport and deposition of particles may occur in all kinds of flows (atmospheric, fluvial, tidal and marine currents; turbidity currents; snow avalanches and, of particular interest here, pyroclastic density currents). As all clastic sediments have been transported and deposited, these processes are fundamental. They shape the landscape, deplete some areas of their soil and yield vast sedimentary deposits elsewhere (covering 70% of the Earth surface). Ripples and dunes form from the cm to the km scale, in aqueous, aeolian and even extraterrestrial environments.

Particle motion in a fluid can be understood as occurring via three main conceptual transport mechanisms: 1) rolling/creep occurring when particles move without leaving the bed, 2) saltation consisting of one or several particle jumps and 3) suspension, where the fluid turbulence fully supports the clasts that therefore exhibit no interaction with the ground.

1.2. Pyroclastic density currents

During explosive volcanic eruptions as well as catastrophic lava-dome collapses, newly-formed particles (pyroclasts) can be transported down the volcanic edifice as dilute particulate density currents, supported by a fluid phase consisting of a mixture of volcanic gas and entrained air (Carey, 1991; Druitt, 1996). Those pyroclastic density currents (PDCs) can flow at hundreds of km/h at temperatures of several

* Corresponding author. Tel.: +49 89 21804272; fax: +49 89 21804176.
E-mail address: g.douillet@min.uni-muenchen.de (G.A. Douillet).

http://dx.doi.org/10.1016/j.jvolgeores.2014.03.011

hundred °C). They thus pose a threat to local populations and infrastructure and can drastically alter the environment (Tanguy et al., 1998). As with any particle-laden flow, dilute PDCs can produce a range of sedimentary structures, including dune bedforms, erosive planes and massive deposits (Branney and Kokelaar, 2002; Douillet et al., 2013a). From a sedimentological point of view, PDCs can be classified based on the processes occurring at their base. Branney and Kokelaar (2002) defined four different kinds: granular, fluid-escape, tractional or fallout-dominated flow boundary zones. Where tractional processes can be inferred from the deposits, generally by the presence of cross-stratification (Douillet et al., 2013b) and a granulometry dominated by ash and lapilli (i.e. particle diameter <6.4 cm, Walker, 1971), particles are believed to undergo transport driven by the fluid phase down to the base of the flow. Each individual particle was thus subject to rolling, saltation and direct fall before deposition. From a theoretical point of view, dilute PDCs are regarded as turbulent, density-stratified, convecting gas-particulate flows (Valentine, 1987; Burgisser and Bergantz, 2002). Because of their opaque and hazardous nature, the internal processes are largely derived from direct observation during their flow and therefore much of our understanding must come from detailed analysis of their deposits. This situation creates a significant role for appropriate laboratory measurements in order to infer insights into flow conditions from the sedimentary record.

1.3. Wind-blown saltation

Saltation is a fundamental transport mechanism on a wind tractional flow boundary, typically accounting for 75% or more of the total mass transport (Bagnold, 1941). Moreover, since suspended particles do not interact with the bed, saltation is also the main mechanism of energy transfers between the flow and the bed (Owen, 1964). Even creeping/rolling particles indirectly extract energy from the wind flow via impacting saltating particles that transfer a fraction of their forward momentum (Bagnold, 1941; Merrison, 2012). Thus, saltation is the main process occurring at a tractional bed interface with particle transport.

Close to a rough boundary, small-scale turbulence generates a mixed layer where the shear stress (τ) can be assumed constant:

$$\tau = \rho u^{*\wedge} 2 \quad (1)$$

with u^* (m/s), is a parameter called the shear (or friction) velocity and ρ the air density. Since the observation scale is much larger than the turbulent time scale, one can parameterize the shear stress by an eddy diffusivity, the size of which is proportional to the distance from the surface (Vallis, 2006, pp. 409–413; Durán et al., 2011):

$$\tau = \rho u^{*} \kappa z dU_z/dz \quad (2)$$

with U_z the average streamwise velocity component. The Von Karman constant κ generally has the value 0.4. Combining Eqs. (1) and (2), we get $dU_z/dz = u^*/\kappa z$, which integrates to define the logarithmic boundary layer known as the "Law of the Wall":

$$U_z = u^* \ln(z/z_0)/\kappa \quad (3)$$

z_0 (dimension of a length) is an integration constant called the aerodynamic surface roughness length (Garratt, 1992). It corresponds to the conceptual height above the bed where the wind speed extrapolated from Eq. (3) decreases to zero (the rougher the bed the larger the value of z_0). Whereas u^* is related to the velocity gradient of the wind-speed profile (slope of the logarithmic profile), z_0 relates to the roughness of the bed and those two parameters together completely define a logarithmic boundary layer. Other expressions of a velocity profile are available to account for secondary effects, but the logarithmic expression is recommended for evaluating shear velocities (see Bauer et al., 2004 and references therein).

For a dynamically fully rough wind over a fixed sand surface composed of uniform grains, Bagnold (1941) found empirically that:

$$z_0 = D_p/30 \quad (4)$$

where D_p is particle diameter. For non-uniform sand, D_p is replaced by D_g being some linear measure of the basal roughness elements (usually 2^*D_{50} or D_{90} where the subscript refers to the percentage of the population that is finer than the indicated size, Church et al., 1990; Nikuradse, 1933; Bauer et al., 2004 and references therein). Note however that for a saltating bed, z_0 slightly depends on u^* (e.g. Owen, 1964; Rasmussen and Mikkelsen, 1990; Sherman, 1992; Rasmussen et al., 1996; Durán et al., 2011).

Conceptually, five forces act on a clast subjected to a flow (Durán et al., 2011; Merrison, 2012): 1) drag force depending on particle shape and the flow speed, parallel to flow direction; 2) lift force depending on particle shape and driven by the pressure difference between the base and the top of the particle, (i.e. shear velocity), perpendicular to the bed; 3) torque force depending on particle shape and driven by the speed

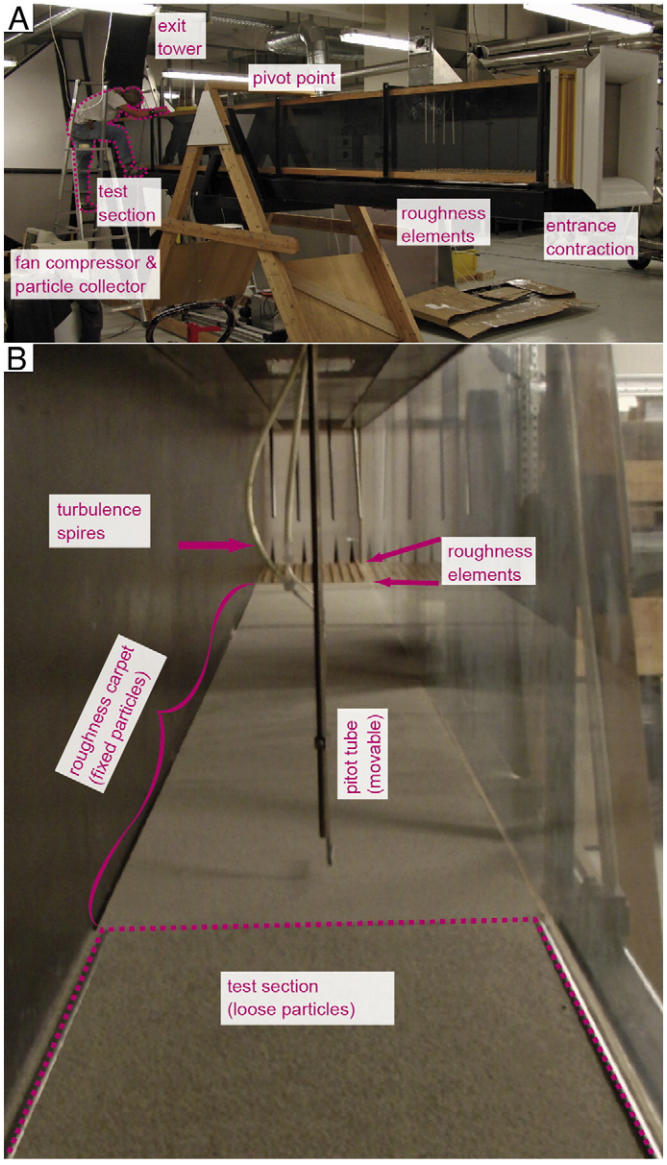

Fig. 1. Wind tunnel used in the study. A) View from the outside with the different sections. Note the pivot point that permits inclination. B) Inner view with the different sections (particles are 1–2 mm pumice). Note: loose bed in front and corresponding roughness carpet in the back.

difference between the base and the top of the particle, (i.e. shear velocity), induce a rotation; 4) adhesive forces including electrification, and other effects, linearly dependent on grain diameter, and other unidentified parameters, active on the contact points; and 5) gravitational forces depending on the density and volume of the particles.

Below a threshold shear velocity, the drag and lift forces are insufficient to counteract the weight of the particle and no motion occurs.

The fluid static saltation threshold ($SST - U^*_0$) is the threshold where particles start to move in saltation under the fluid shear stress alone (Durán et al., 2011). It is characterized by the minimal speed profile that initiates saltation of particles from a state of repose. For large particles such as sand-sized material, adhesive forces can be largely neglected, and the threshold is dominated by gravitational and torque forces (i.e. motion will be initiated by brief rolling leading to saltation, Durán et al., 2011; Merrison, 2012). The critical shear stress for transport depends on the drag coefficient, the vertical velocity profile near the bed and the characteristics of the particle bed. Bagnold also defined the impact (dynamic) threshold for saltation which is the minimum shear stress (speed profile) for which an already saltating bed can be maintained in saltation. The distinction is required by the fact that there is an amount of energy that must be transferred to initiate saltation, but once saltation has begun, the impacting particles will transfer part of their energy to particles in repose, possibly ejecting new particles (known as the splashing effect, Creyssels et al., 2009; Kok and Renno, 2009; Durán et al., 2011).

1.4. State of the art

The first physically-based intensive studies of wind-blown sand transport were conducted by Bagnold (1941). Iversen et al. (1976) measured the SST for blowing wind over different types of clast shapes, grain sizes and densities. Iversen and Rasmussen (1994, 1999) investigated the effect of bedslope on saltation threshold and mass transport. Those experiments provided the motivation for the present work, to provide an erosion threshold for pyroclasts that can be compared to field-based grain size data. A large number of studies on grain sizes of pyroclastic deposits are available (e.g., Sparks, 1976; Walker, 1984), yet these data remain underexploited in terms of the quantitative relations that might be derived for the flow parameters.

Some efforts have been made to relate field features to quantitative dilute PDC flow parameters related to the boundary layer. The shape of erosive furrows, for example, has been linked to the size of boundary layer eddies and used to derive flow velocities (Kieffer and Sturtevant, 1988). Dilute PDCs are particle-laden flows with dominant fluid–particle interactions and minor particle–particle support. Depending on the transport hypothesis, one of two approaches can be applied to link their deposits to flow parameters: 1) the sediment was emplaced from turbulent suspension transport (suspension criterion) or 2) the sediment was emplaced in a tractional boundary with saltation and thus must have been transported by the fluid-phase turbulent shear at the flow boundary (Shields criterion). The suspension criterion suggests that particles deposited from dilute flows must have been transported in suspension, thus the flow turbulence scales the terminal fall velocity of the transported material (Middleton, 1976; Dellino and La Volpe, 2000). The use of the Rouse number is an alternative formulation of this problem (e.g. Valentine, 1987). However, for deposits of supposedly dilute PDCs, the use of the suspension criterion applied to the coarsest clasts found will lead to unrealistic velocity values if flow density is not taken into account (Sparks, 1983; Walker and McBroome, 1983; Lajoie et al., 1989). Moreover, the settling velocity of pyroclasts is difficult to calculate (Walker et al., 1971; Sparks et al., 1978; Bonadonna et al., 1998; Dellino et al., 2005), thus the suspension criterion requires

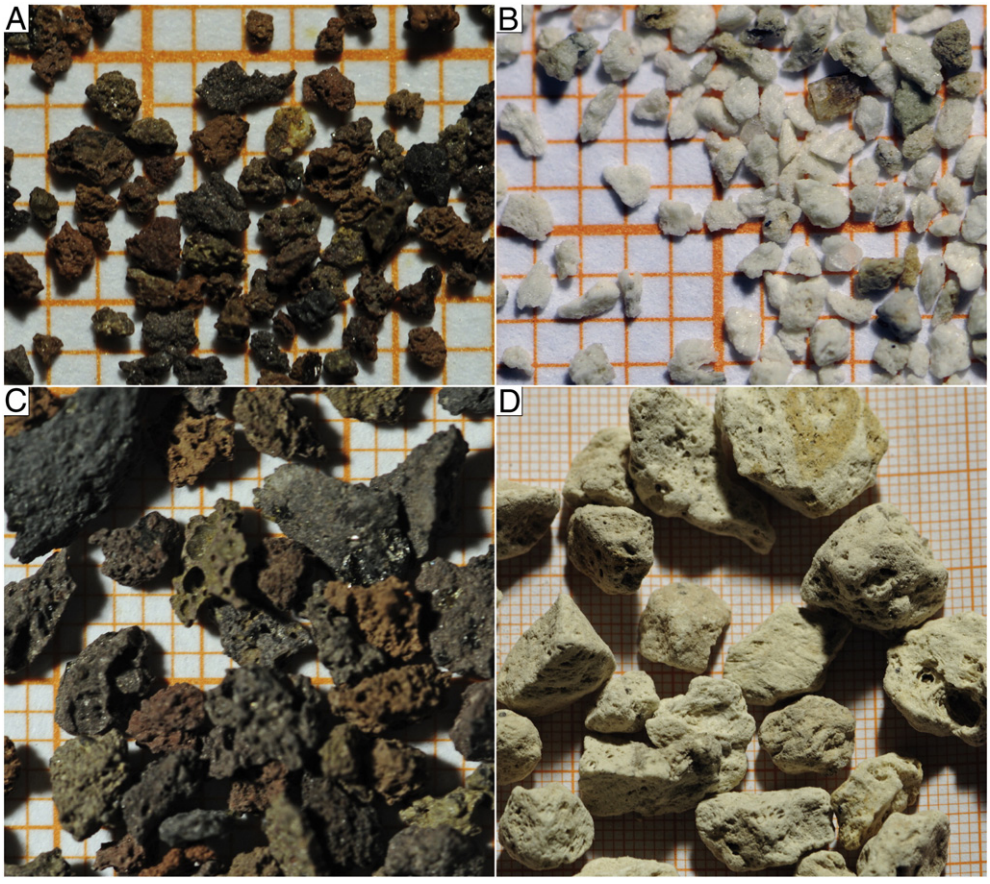

Fig. 2. View of the pyroclasts. Background grid is in mm. Particles: A) 0.5–1 mm scoria; B) 0.5–1 mm pumice; C) 2–4 mm scoria; D) 4–16 mm pumice. Note: vesiculated nature and angular shapes.

the estimation of both flow density and particle terminal fall velocities. On the other hand, the Shields criterion consists of the minimal shearing necessary to onset particle motion (Shields, 1936; Miller et al., 1977). Dellino et al. (2004a) applied the Shields criterion to cross-stratified deposits and the suspension criterion on directly overlying deposits in order to completely constrain the parental transitory flow (with response on the ethics by Le Roux, 2005). They later applied this method to the coarse- and fine-grained modes of the same layer, assuming a bedload and suspension transport for the modes (Dellino et al., 2008). In practice, both methods provide a threshold value for the horizontal shear velocity.

Here, we present a set of wind tunnel measurements at variable bedslope in order to characterize the static saltation threshold and surface roughness for pyroclastic particles of different density and grain size. Under the assumption that PDC deposits reflect boundary layer processes during emplacement, this dataset is well-suited to enhance our quantitative understanding of PDC dynamics.

2. Method

2.1. Wind tunnel measurements

In this study, we used a wind tunnel with adjustable bed inclination (Fig. 1, described by Iversen and Rasmussen, 1994). Because of the sloping possibility, the length is only 6 m and the flow thus needs to be adjusted immediately to the downwind equilibrium. A set of turbulence-generating spires and roughness blocks (on the first 80 cm) are placed at the upstream end of the tunnel. In the following 4 m in downwind direction, a roughness array is created on the bed. The roughness array consists of a board with a flat bed of particles glued on it and a roughness array was prepared for each sample type so that a fully developed turbulent wind profile in equilibrium with each sample type was achieved. The downstream end of the section consisted of a ca. 1 cm thick layer of loose samples on a length of 1 m.

The SST was measured by gradually increasing wind speed (blindly, i.e. without knowing the value) in the tunnel until a small but continuous amount of particles began to saltate at the downstream end of the test section. The observation was performed visually with the help of a laser beam that highlighted saltons. The criterion was that more than one particle would begin to saltate within a 5 s time-window during at least 1 min (thereby ensuring that not only the most unstable particle would move). The wind profile was then recorded at the downstream end of the roughness carpet using a pitot tube connected to a precision manometer. This method was previously applied by Iversen and Rasmussen (1994), who validated their results by comparing them with those obtained in a 15 m-long wind tunnel.

2.2. Particles

In order to evaluate the influence of particle characteristics on their saltation threshold and surface roughness, two kinds of natural pyroclasts from the East Eifel volcanic area (Germany) were used (Fig. 2). Pumice particles from the Laacher See eruption were provided (pre-washed with heavy water and pre-sieved), by ROTEC GmbH & Co. KG (Mühlheim–Kärlich), scoriaceous fragments of a porous lava flow ("Schaumlava") were provided by Paul Link GmbH & Co. KG (Kretz). Wet mechanic sieving in one ϕ intervals was performed (0.125 mm–16 mm).

Matrix densities were measured by Helium pycnometry (Ultrapyc from Quantachrome) utilizing ca. 30 g of particles from each fraction (Fig. 3A). Density is stable between the different size fractions with an average of 2.5 g/cm^3 and 1.4 g/cm^3 for the scoria and pumice particles, respectively. The pumice particles were found to float on water for several days.

Four shape parameters were derived from measurements of hundreds of single particles with a Retsch Camsizer: sphericity (avg. 0.81 ± 0.07), symmetry (avg. 0.87 ± 0.02), aspect ratio (avg. 0.68 ± 0.04) and convexity (avg. 0.98 ± 0.01) (Table 1, Fig. 3B–E). All samples show similar values. This similarity might be a consequence of the large number of particles analyzed for each sample type (>500).

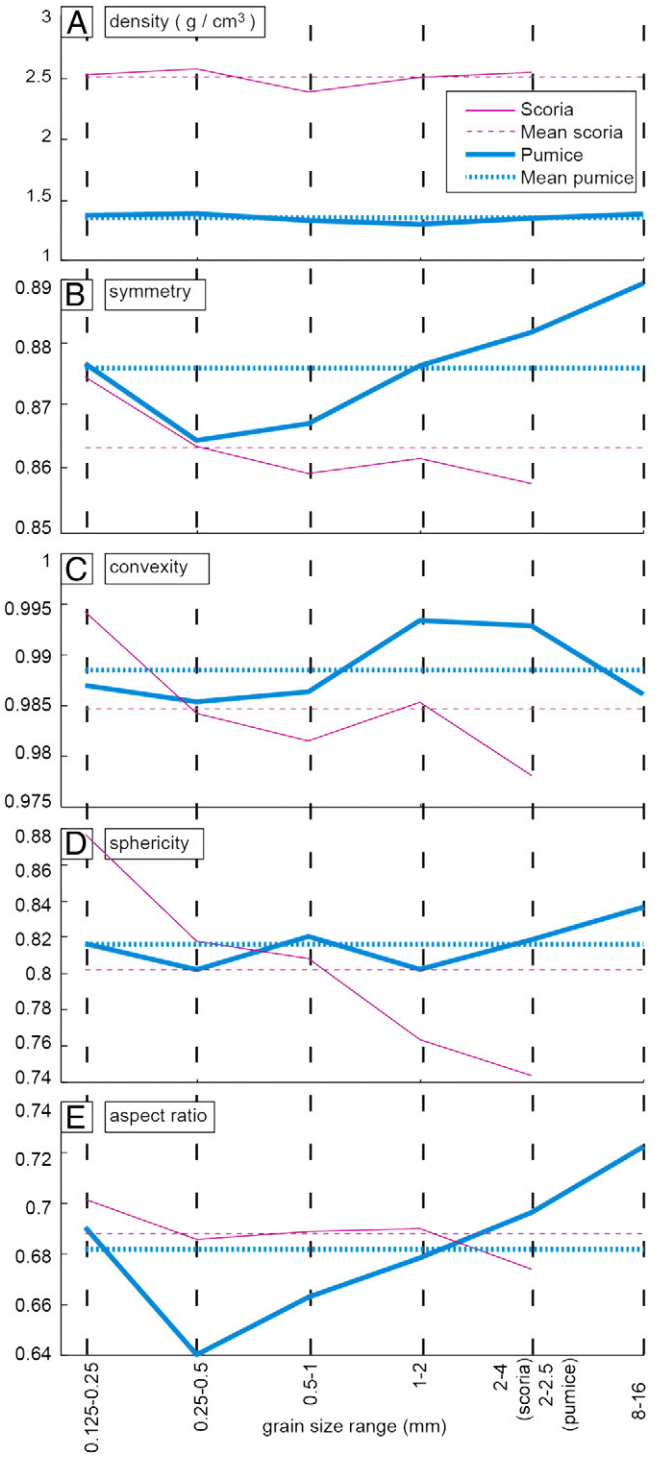

Fig. 3. Averaged particle parameters by samples. A) Density, B) to E) shape parameters.

3. Data

3.1. Static saltation threshold

Wind profiles recorded at the SST at zero bed slope show typical log-linear turbulent curves following the law of the wall (Fig. 4). Repeated

Table 1
Shape parameters for all particle types derived from averaged Camsizer measurements and densities.

Grain size (mm)	Sphericity	Symmetry	Aspect ratio	Convexity	Density ($kg \cdot m^{-3}$)
Scoria					
0.25–0.125	0.8767	0.8745	0.7015	0.9942	2531
0.5–0.25	0.8177	0.8635	0.6858	0.9841	2580
1–0.5	0.8081	0.8593	0.6889	0.9814	2391
2–1	0.7634	0.8616	0.69	0.9852	2511
4–2	0.7435	0.8576	0.6741	0.978	2552
Mean	0.8019	0.8633	0.6880	0.9846	2513
Pumice					
0.25–0.125	0.8164	0.8766	0.6906	0.9869	1383
0.5–0.25	0.802	0.8645	0.6405	0.9853	1398
1–0.5	0.8203	0.8671	0.6631	0.9863	1340
2–1	0.8022	0.8763	0.6785	0.9933	1309
2.5–2	0.8186	0.8816	0.6964	0.9928	1359
16–8	0.8365	0.8893	0.7222	0.986	1394
Mean	0.8160	0.8759	0.6819	0.9884	1364

Table 2
Results of the windtunnel measurements. Abbreviations: GS up/low: upper and lower grain size range; u^*: shear velocity; ⊙: threshold Shields number; z_0: surface roughness length; v_{10cm} and v_{100cm}: extrapolated velocity at 10 and 100 cm above the bed, respectively, following Eq. (3); Rep.: number of repetition of the whole measurements used for averaging.

GS up (mm)	GS low (mm)	u^* (m/s)	⊙	z^0 (mm)	v^{10cm} (m/s)	v^{100cm} (m/s)	rep.
Scoria							
0.25	0.125	0.2046	0.1728	0.1765	4.86	6.01	1
0.5	0.250	0.2856	0.1386	0.2395	6.57	8.18	2
1	0.5	0.4596	0.1932	0.5205	9.7	12.28	3
2	1	0.6574	0.3142	2.9249	11.12	14.81	2
4	2	0.6852	0.1887	3.1374	11.47	15.32	1
Pumice							
0.25	0.125	0.0629	0.1042	0.1563	1.51	1.87	2
0.5	0.25	0.0546	0.0466	0.0793	1.41	1.71	3
1	0.5	0.0979	0.0381	0.1596	2.35	2.9	1
2	1	0.4359	0.1545	1.4294	7.93	10.38	3
2.5	2	0.4675	0.1845	2.5799	8.05	10.67	2
16	8	0.6808	0.0835	8.0416	9.83	13.66	1

measurements show consistent results, demonstrating the reliability of the set-up. Shear velocities were estimated from log-linear best-fit regressions of the data (Eq. (3), Table 2). Estimates of surface roughness lengths were derived directly from the best-fit regression parameters generated for estimating shear velocities (as the height where the profile crosses the zero velocity line, Table 2).

The shear velocities for the SST are compared to standard curves for different clast densities and shapes (Fig. 5 from Iversen et al., 1976). Both scoria and pumice samples of all grain sizes plot within the field for round particles of similar densities, thus the SST seems to be little affected by the high angularity and other specificities of the pyroclasts.

The Shields number (⊙) is often used as a dimensionless criterion for motion:

$$\odot = \rho_f (u^*)^2 / \left(\rho_p - \rho_f\right) g\, D_p \qquad (5)$$

Given all the values measured for the experiments, we calculated the threshold Shields number (Fig. 6). Values are in the smallest range of measured data, as expected for particles of large size (as defined in the aeolian research context—100 s μm). Indeed, the Shields number is a parameter based upon a simple model including only gravity and a lift type force, whereas for large grains, detachment occurs through

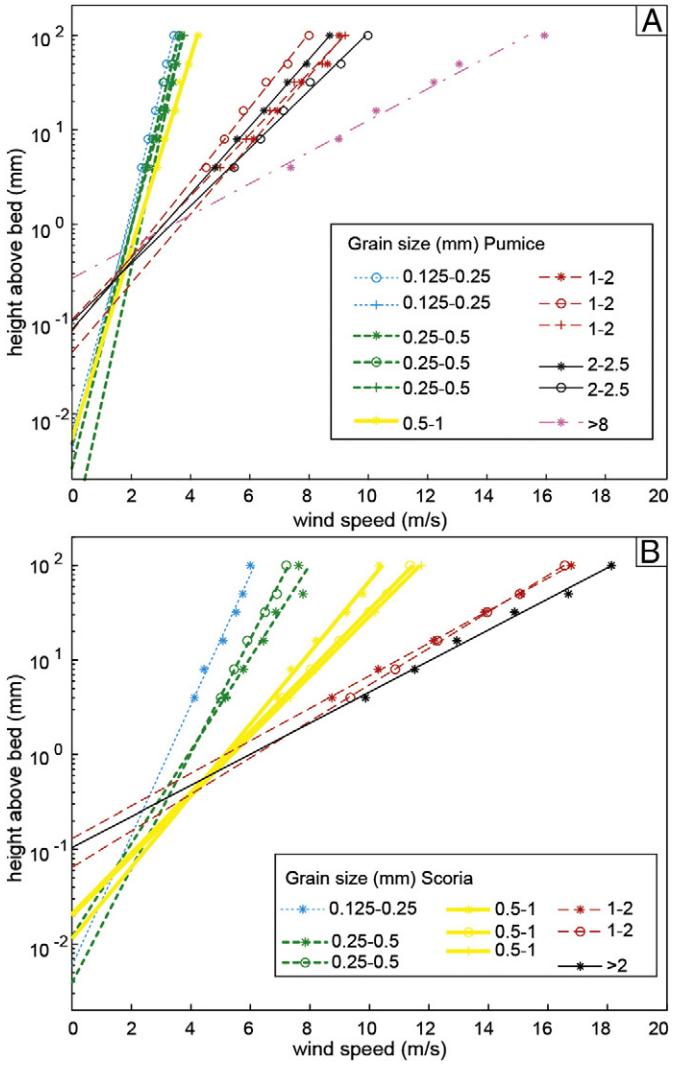

Fig. 4. Speed profiles at SST. Points are measurements, lines are logarithmic fits. Samples by colors, repeated samples have the same color. A) Pumice samples, B) scoria samples.

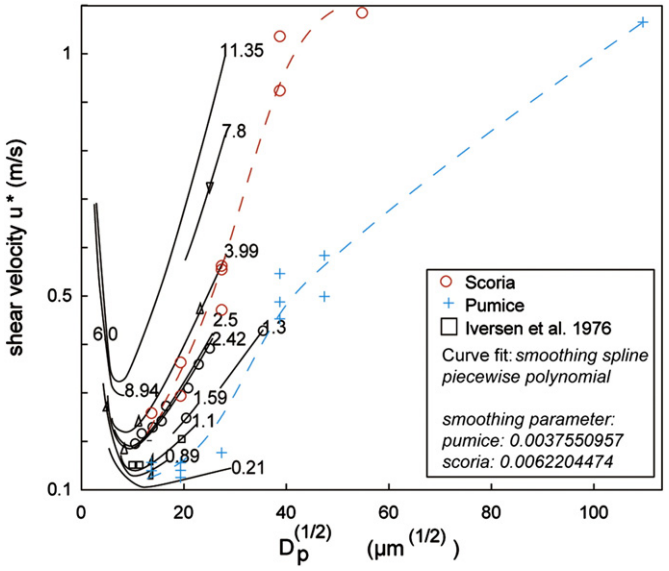

Fig. 5. Saltation threshold shear speeds as a function of grain diameter (square root). Data are compared to results from Iversen et al. (1976) in black, with numbers indicating densities of the studied material.

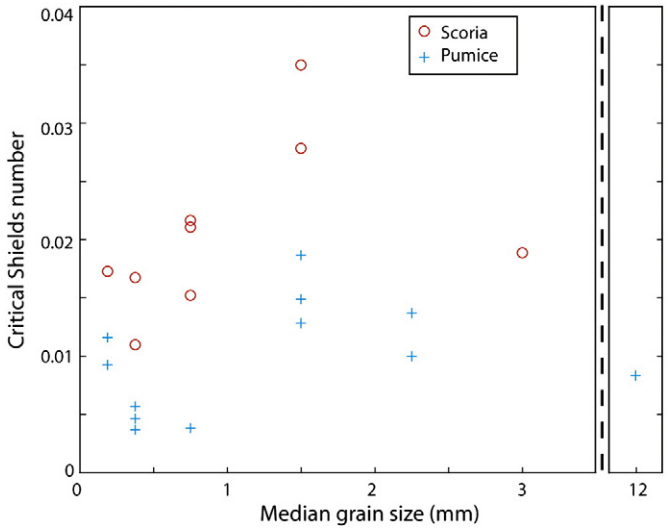

Fig. 6. Static threshold Shields numbers calculated from Eq. (5) and the measurement results for sample type and grain size. Values in table 3.

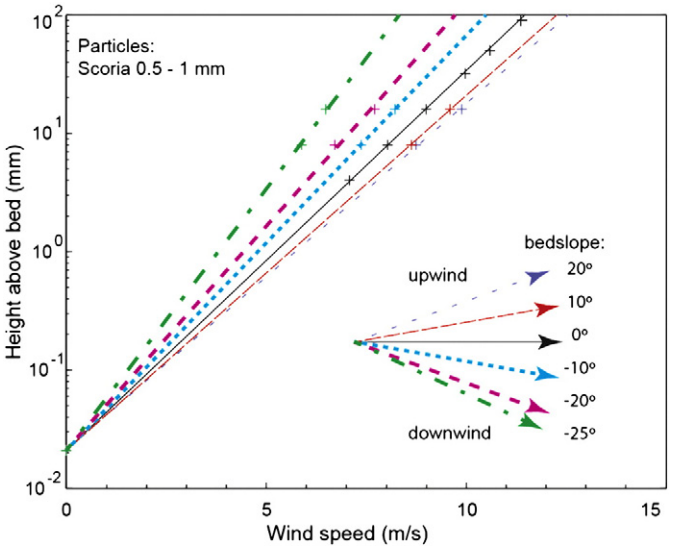

Fig. 8. Example of the slope influence for the 0.5–1 mm scoria samples. Color coding indicates the bedslope. Surface roughness lengthscale is fixed to the no-slope value.

rolling, which has only a weak dependence upon size. The Shields number might thus be inappropriate for particle transport in PDCs.

3.2. Surface roughness

Empirically, it was observed that the surface roughness length roughly obeys Eq. (4), thus solely depending on grain characteristics. There is some scatter in the extrapolated surface roughness length for the pyroclasts (Fig. 7). While the larger clasts fit reasonable well in the range expected some of the values obtained for the smaller pumice particles (<1 mm) are lower than expected. This may be due to a larger measurement uncertainty for fines: the lowest measurement height is fixed by the size of the sensor, and extrapolation to the zero wind speed must thus be longer for the smaller speed gradient above the finest particles.

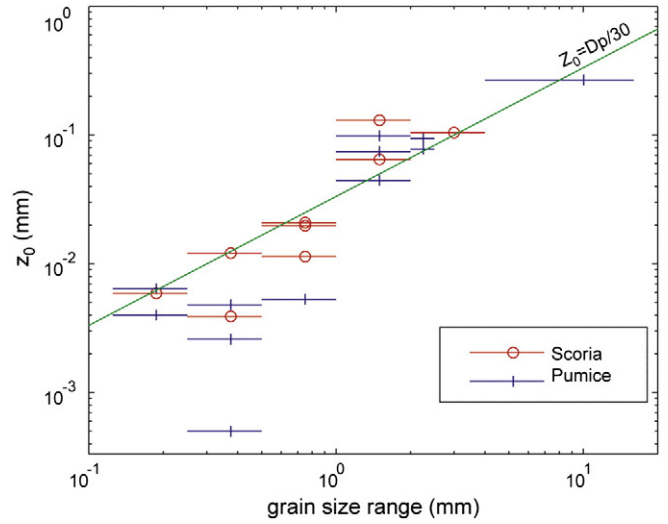

Fig. 7. Surface roughness lengthscale (z_0) as a function of grain size range. The horizontal bars indicate the grain range of each sample. Green line follows Eq. (4) with the mean diameter.

3.3. Inclined profiles

The SST was similarly observed for measurements with an inclined bed and velocities measured at two different heights. Since the particles for horizontal and inclined tests are the same, the surface roughness lengths were assumed to be unaffected by inclination and taken as those from the zero-slope results. This assumption was previously verified on the same set-up by Rasmussen et al. (1996). The SSTs are affected only because gravity forces act with or against the wind influence (Fig. 8, Table 3). In order to compare the threshold values and eliminate systematic parasitic effects, sloping results are normalized to the zero-slope SST (Fig. 9). A discussion on the effects of slope on the SST is available in Iversen and Rasmussen (1994) for sand particles. In our experiments, the SST can be increased by up to 82% when the slope acts against flow direction compared to the minimum (downflow) results, and is on average greater by 50%. Both sample types exhibit the same trend and no clear trend regarding grain size was discerned.

Table 3
Values of shear velocity for different bedslope angles and all samples. Positive bedslope value: slope acts against flow direction. GS up/low: upper and lower grain size range (mm).

	Angle (°)	20	10	0	−10	−20	−25
GS up	GS low	u* value	u* value	u* value	u* value	u* value	u* value
Scoria							
0.25	0.125	0.2756	0.2731	0.2584	0.2223	0.2065	0.1836
0.50	0.25	0.3892	0.3775	0.3631	0.3250	0.2702	0.2682
0.50	0.25	0.3362	0.3298	0.2941	0.2725	0.2402	0.2266
1.00	0.50	0.5526	0.5232	0.4714	0.4355	0.3451	0.3316
1.00	0.50	0.6076	0.5933	0.5547	0.5077	0.4712	0.4027
2.00	1.00	1.1204	1.0669	1.0361	0.8365	0.7400	0.6162
2.00	1.00	1.0647	1.0290	0.9240	0.9029	0.8044	0.6894
4.00	2.00	NO DATA	1.2409	1.0846	1.0421	0.9522	0.8553
Pumice							
0.25	0.125	0.1612	0.1560	0.1395	0.1416	0.1305	0.1243
0.50	0.25	0.1315	0.1266	0.1253	0.1132	0.1080	0.0959
1.00	0.50	0.2139	0.2073	0.1765	0.1748	0.1594	0.1456
2.00	1.00	0.4938	0.4851	0.4877	0.4474	0.3982	0.3482
2.00	1.00	0.5457	0.5362	0.4528	0.4567	0.3979	0.3713
2.5	2.00	0.5996	0.5879	0.4990	0.5117	0.4517	0.4093

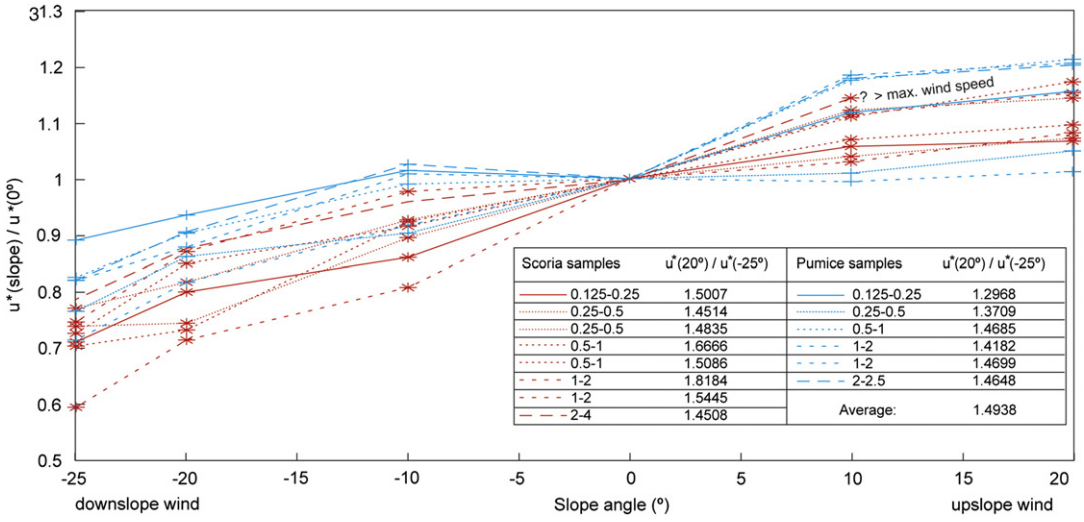

Fig. 9. Influence of slope on the static saltation threshold normalized by the no-slope threshold. Inlet table gives the ratio between maximal downslope and upslope results. Results presented for both scoria and pumice particles.

4. Discussion

4.1. Considerations for use

A link between pyroclast grain size and the associated SST has been measured with a wind tunnel in order to serve as a reference for field studies. Nevertheless, the use of the results is not straightforward and requires careful consideration. The data presented here are for pure wind, without particle load and they are only relevant in the vicinity of the bed interface. Even very dilute PDCs are likely to be highly loaded in particles saltating or in suspension, with various grain sizes.

4.1.1. Boundary processes

Our data relate to near bed boundary processes at the sedimentation interface and the surface roughness lengths are for wind exposed to grain-scale topography. We refrain from extrapolation to a larger part of a PDC's thickness.

A simple logarithmic profile is valid in the vicinity of the bed, but it is most likely that the basal roughness elements influencing on the turbulence for a whole PDC consist of trees, large bedforms and geomorphological features (Dellino et al., 2004b). In that case, an additional term "d_0" (displacement length) is needed in Eq. (3) to correct for surfaces with large roughness elements that account for a considerable part of the wall friction (Grimmond and Oke, 1998):

$$U_z = u^* \ln((z-d_0)/z_0)/\kappa$$

Even so, the law of the wall is valid in the vicinity of the boundary only, and a velocity profile is likely to reach a freestream velocity or follow some Kolmogorov model in its outer parts (defect layer). Dilute PDCs are complex, with density stratification, convection, and flow regime changes interacting with turbulent eddies at a range of scale (Valentine, 1987; Burgisser and Bergantz, 2002; Andrews and Manga, 2012), so that our data should only be used as an instantaneous shear threshold near the bed, that is intermittently reached via the flow's large-scale turbulence.

4.1.2. Flow density

For a given speed, flow density and shearing are positively correlated. This needs to be addressed, especially in the PDC context, because: 1) elevated temperatures lead to decreased gas densities and 2) the particle volumetric concentration can increase the bulk density of the flow (Boudon and Lajoie, 1989). Consequently, the shear velocities presented here need to be converted in flow velocities by carefully taking into account the density of the flow. Table 4 summarizes the flow density for different concentrations and air at 25 °C (ambient air), 100 °C (liquid water limit), 230 °C (wood scorches—Bradbury, 1953), 270 °C (wood carbonizes—Lullin, 1925), and 450 °C (highest temperature encountered in the literature by the authors, Lacroix, 1904).

Air density depends upon temperature as:

$$\rho_{air} = M_{mol}P/(RT) \quad (6)$$

with $M_{mol} = 0.029$ kg/mol the molecular mass of air, $R = 8.314$ J/(mol·K) the ideal gas constant, P taken at 1.013 hPa the atmospheric pressure, and T the temperature in Kelvins.

The particle volumetric concentration is probably the most difficult value to assess. Doronzo and Dellino (2011) used a value of 3.7% at 1 m above the ground for their numerical simulations, a value based on deposit analysis and experiments (Dellino et al., 2008). However, probably only the finest, suspended fraction of the particles can be considered as increasing the density of the fluid whereas larger particles are more likely to be in (partial) interaction with the ground contact zone and participate in boundary layer saturation (Simons et al., 1963). Doronzo and Dellino (2011) used a grain size distribution containing 4.6% of particles with a diameter of 63 μm, the remaining 95.4% with a diameter of 1.4 cm and above. We can thus also consider the case where only particles of 63 μm and less contribute to the flow density.

Considering,

$$\rho_{flow} = C\rho_p + (1-C)\rho_f \quad (7)$$

with C the particle volumetric concentration.

Table 4 summarizes the different densities depending on temperature and particle volumetric concentration. It clearly shows the dominant influence of particle concentration over temperature. Although density of a pure wind can double in the temperature range of PDCs,

Table 4
Values of flow density ($kg \cdot m^{-3}$) calculated for different temperatures (T(°C)) following Eq. (6) and volumetric particle concentrations (C(%)) following Eq. (7). For particle concentrations above 0, the value is given for a particle density of 1300 and 2500 $kg \cdot m^{-3}$.

T(°C)\C(%)	0	0.17	1	3.7
25	1.19	3.39/5.43	14.17/26.17	49.24/93.64
100	0.95	3.15/5.20	13.94/25.94	49.01/93.41
230	0.7	2.91/4.96	13.70/25.70	48.78/93.18
270	0.65	2.86/4.90	13.64/25.64	48.73/93.13
450	0.49	2.70/4.74	13.48/25.48	48.57/92.97

particle concentration mostly governs the flow density and leads to increases with a factor of 200 between our extreme examples. As a comparison, Brand and Clarke (2012) used densities of 3, 7 and 11 kg/m^3 on their analysis based on Wohletz (1998).

Given that the SST is a shearing threshold (thus the threshold parameter is τ and not u^*), it appears from (Eq. 1) that the shear velocity, (and so the slope of the velocity profile) at a given shear stress is controlled by the root of the bulk flow density, so that:

$$u^*(\rho_i) = u^*(\rho_0)(\rho_0/\rho_i)^\wedge(1/2) \quad (8)$$

As a first approximation, the values of SST can thus simply be corrected by taking an adequate flow density, and the new shear velocity applied to calculate the wind profile. Note, however, that the saltation threshold increases itself up to a factor 2 due to the particle-to-fluid density-ratio in a more complicated manner, probably as an effect of the relative energy with which particles interact with each other (Iversen et al., 1987).

4.1.3. Saturated flux

A saltating bed transports a given flux of particles, depending on the wind profile (Zheng et al., 2004; Creyssels et al., 2009), or in other terms, it reaches a maximal transport capacity, i.e. a saturated flux (Durán and Hermann, 2006). The particle concentration and its effects on entrainment and erosion capability are especially relevant for dilute PDCs with load greater than aeolian transport.

During saltation, the moving grains extract momentum from the air, and so the shear stress in the saltation layer can be divided into the grain-borne and air-borne shear stress. As long as the saturation flux is not reached, more grains are entrained, and a transfer from air-borne to grain-borne shear stress occurs. At saturation, no additional grains can be put in motion and the air-borne shear stress is reduced just below the saltation threshold (Owen, 1964; Iversen and Rasmussen, 1999; Durán et al., 2011). Several models have been suggested for saturated transport (Andreotti, 2004; Zheng et al., 2004; Durán and Hermann, 2006; Durán et al., 2011 – chap 4.3 – and references therein), and are beyond the scope of the data presented herein. In most models, even if the velocity profile *above* the saltation layer could indicate that the saltation threshold is exceeded, no additional particles will be entrained if the fluid *in* the saltation layer has already reached saturation. Saturation would be an equilibrium state with continuous exchange of particles between the bed and fluid phase (entrainment and deposition) but no net erosion. Saturated transport is a fundamental aspect for decelerating dilute PDCs, whose total transport capacity will reduce downflow.

Experiments on the influence of settling particles on the formation of cross-laminations in aqueous flows seem to indicate that 1) cross-lamination is inhibited for antidunes but not for lower stage bedforms (Arnott and Hand, 1989), 2) high deposition rates from the suspended load in density currents will produce poorly-graded deposits (Sumner et al., 2008) and 3) high concentrations of fine particles ease the formation of cross-lamination (Simons et al., 1963). Several studies have suggested that a tractional boundary is inhibited by high basal clast concentration, which is thought to account for fine-grained, massive or faintly stratified beds (Branney and Kokelaar, 1997; Brown and Branney, 2004; Sulpizio et al., 2010). The current lack of knowledge on the saturated flux and the uncertainties of application it entails should be kept in mind when applying the present dataset to PDCs.

Finally, the presence of particles landing from the upper parts of a PDC on the ground contact zone may, in some cases, induce mobilization of the bed that would otherwise not move. Indeed, particles falling and bouncing from the upper part of the flow are an input of energy to the interface and might eject other particles during impact, like the splashing effect for saltons. As such, the dynamic saltation threshold (the speed to maintain an already saltating bed in saltation, Iversen and Rasmussen, 1994) might provide results closer to what corresponds to a PDC boundary with landing particles from the upper part. The ratio of dynamic to static threshold is about 0.7 (Iversen and Rasmussen, 1994).

4.2. Application to PDC deposits

4.2.1. Cross-bedding type

At least three types of cross-bedding can be recognized in PDC deposits: 1) "partially erosive cross-lamination", 2) "differential draping laminations", and 3) "non-laminated cross-bedding" (Branney and Kokelaar, 2002; Douillet et al., 2013a, 2013b; Fig. 10).

The "partially erosive cross-laminations" consist of all those kinds of bedforms that show truncations, e.g. stoss-eroded dune bedforms, the so-called "chute and pool" type of bedding, or any erosive plane (Fig. 10A). In such cases, it can be inferred that previously deposited particles have been remobilized. Provided that it can be inferred that a dilute flow eroded the former deposits, one can relate the grain size of the deposits to the associated SST as a minimum value. Indeed, no particles would move below the threshold.

The "differential draping laminations" consist of those bedsets aggrading on both sides of a bedform in an asymmetrical manner (e.g. climbing dunes and stoss-depositional dune bedforms, Fig. 10B). Recent interpretation has suggested that stoss-aggrading dune bedforms are produced by a transitional process between direct fallout and tractional current in dilute PDCs with preferential draping on the stoss side but little tractional component (Douillet et al., 2013b). In such a case, the SST would thus represent an upper limit for the formation of dune bedforms by differential draping, since passing the threshold would imply a major influence of tractional processes.

Finally, for the "non-laminated cross-bedding" type, it should be stated clearly that not all cross-bedding within PDC deposits has been deposited from dilute PDCs with a tractional boundary. If the smallest strata forming a sedimentary structure are more than a few mm thick and indeed represent thin, massive layers, then caution must be taken during interpretation (Fig. 10C). Such layers might be emplaced from a granular-based flow boundary, possibly dense pyroclastic flows. The same applies for very diffuse laminations (Fig. 10D), where the structure can represent a deposit from a dilute PDC with a high particle concentration at its base (traction carpet, Sohn, 1997). Even if the fluid phase dominated most of the flow, particles might deposit with none or all diffuse lamination because high deposition rates or bedload transport would completely saturate the boundary, inhibiting cross-stratification. In that case, even if the SST is reached, it cannot affect the sediment bed, because a thin traction carpet would "reptate" between the fluid phase and the actual deposit. This case might to some extent be similar to the model by Andreotti (2004).

4.2.2. Stoss-aggrading dune bedforms

The results of the inclined-bed measurements bring a new view on the formation of stoss-aggrading dune bedforms that have successive crest migrating upstream. These structures are typical for the dilute PDC record (Fig. 10B). They are often observed on the steep flanks of volcanoes and they exhibit both stoss and lee face angles dipping from 0 to more than 35° to the horizontal (Douillet et al., 2013b). Typical wind-blown dunes on the other hand are relatively simpler systems where particles are eroded and transported on a gentle stoss side, and deposited on the steeper lee side at the repose angle. The genesis of stoss-aggrading dune bedforms produced from PDCs has been variously interpreted as antidunes (indicating stationary gravity waves, Fisher and Waters, 1969; Crowe and Fisher, 1973), as a plastering effect (indicating liquid water content in the flow, Allen, 1982), as the result of en-masse deposition of individual pulses (Sulpizio et al., 2007) or as a differential draping effect due to high direct sedimentation from the suspended load (Douillet et al., 2013b).

From the inclined measurements it appears that, in order to produce erosion on the stoss side and deposition on the lee side, as is the case for

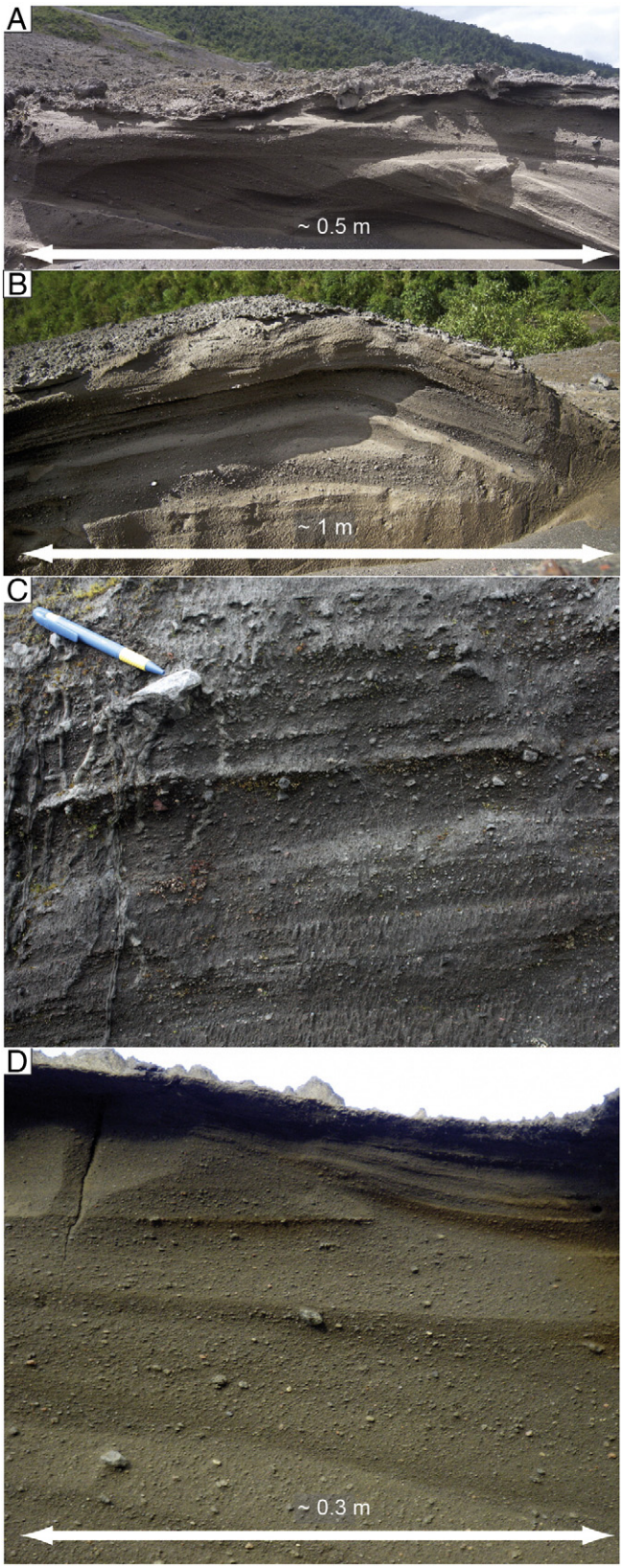

Fig. 10. Examples of PDC deposits. A) truncated laminations covered by planar lamination. B) Stoss-aggrading dune bedform showing differential draping. C) Cross-bedding made from thin layers rather than laminae. D) Very diffuse lamination. All outcrops from the deposits of the 2006 eruption of Tungurahua volcano (see Douillet et al., 2013a, 2013b).

typical dunes, the shear velocity must be more than 50% higher on the stoss face for PDC bedforms (difference between upslope and downslope wind threshold—inset in Fig. 9). Unless a detachment eddy is produced above the lee face, it however seems unlikely that such difference would occur between the stoss and the lee side. This rules out antidunes (i.e. bedforms related to stationary gravity waves, Prave, 1990) as an interpretation. For dune bedforms produced by traction in pure fluids (aeolian wind, water flows), no deposition can occur on the stoss side, because material is not available from the flow directly, it first needs to be put in transport (eroded from the stoss side), and only thereafter can be deposited (on the lee side). In the case of dilute PDCs however, the sediment is present everywhere in the flow, settling from the upper parts of the PDC, and thus, as long as the 50% shear velocity decrease between the stoss and lee are not satisfied, stoss aggradation will be more important than lee aggradation. Any shear difference lower than 50% would not permit to produce downstream migrating bedforms, and erosion would be less pronounced on the stoss than the lee side (or, under aggrading conditions, there would be more stoss aggradation). This can explain the widespread occurrence of stoss-aggrading bedforms in PDCs. Moreover, this process is actually not limited to PDCs, but includes other particle-laden flows and particulate density currents (sediment-laden hyperpicnal flows, turbidity currents), and indeed, similar bedforms occur in their deposits (Douillet et al., 2013b; Lang and Winsemann, 2013).

4.2.3. Example of flow velocities inferred from PDC deposits

We use field observations from the 2006 PDC deposits at Tungurahua volcano (Douillet et al., 2013a, 2013b) as an example of a simple approach: The presence of slightly burned wood fragments is taken as a hint for a flow temperature of 270 °C. Abundant aggrading cross-bedding suggests high particle concentration but within a tractional boundary zone (particle concentration of 3.7%). Scoria and dense clasts form most of the deposits (particle density taken 2500 kg/m^3). This corresponds to a flow density of 93.13 kg/m^3. Freshly emplaced loose cross-stratified bedsets containing laminations with particles up to ca. 1 to 2 mm diameter have been eroded repeatedly. For a pure wind at ambient temperature this would correspond to a shear velocity of 0.6574 m/s, and a velocity of 11.12 and 14.81 m/s at 10 and 100 cm above the bed, respectively (Table 2). Correcting for the flow density indicated above, the shear velocity becomes 0.0743 m/s and the velocities become 1.26 and 1.67 m/s at 10 and 100 cm above the bed, respectively. This corresponds to a decrease of one order of magnitude, leading to very low shear velocities for entrainment of particles.

The measured (and corrected) SST shear velocities and near bed flow velocities obtained from our study are thus at the lowermost limit of velocities usually inferred for dilute PDC deposits. Walker (1984) interpreted the grain size and sedimentary structures found within dilute PDC deposits as indicative of weak and slow flows, fully supported by our measurements. One should keep in mind that in order for a sedimentary structure to form, sedimentation should be possible (i.e. if a flow is too fast, it is unlikely to deposit). For example, Brand and Clarke (2012) observed 20 m-long structures interpreted as antidunes, from which they inferred layer-averaged flow velocities of 30–80 m/s. For layers showing a kink in their bedslope angle (interpreted as chute and pool structures) they inferred layer-averaged flow velocities of 52–73 m/s. From our measurements, the near bed velocities at saltation threshold with the flow density they use (7 kg/m^3) for 8–16 mm diam. pumice particles (as we observe from their pictures) would result in a shear velocity of 0.2807 m/s and velocities of 1.73 and 3.30 m/s at 10 and 100 cm height above the bed, respectively (Table 2). For 2–4 mm diam. scoria particles, velocities of 2.37 and 3.95 m/s would be acting at 10 and 100 cm height above the bed, respectively. Above these velocities, the flow should be over-saturated to force deposition or erosion should occur. It is complex to compare layer-averaged velocities with near bed values, but our results bring a new perspective on the *sedimentation* phases of a dilute PDC. We do not exclude fast flow velocities for dilute PDCs, such as the 235 m/s obtained by Kieffer and Sturtevant (1988)

for the Mount St. Helens blast, but as they did, such velocities should only be associated with erosional, and not depositional features.

5 . Conclusion and overview

We performed wind tunnel measurements of the shear velocity at the saltation threshold and the surface roughness length scale for pyroclastic particles. The dataset was measured for different types of particles, different grain sizes and at various slope angles to account for the variety of features observed in the field. Carefully used, the dataset permits linking of field characteristics (the grain size of a sedimentary structure) to quantitative flow parameters (the shear velocity necessary to put the particles in motion). The results also yield the order of magnitude of the shear velocities acting during deposition of PDCs, a valuable input for numerical models.

Several effects have to be taken into account in order to avoid over-interpretation or misuse of the dataset: the effect of the fluid-phase density has to be corrected and the influence of particle concentration and settling has to be addressed. Different scenarios can be envisaged and careful description and interpretation of the sedimentary record remains fundamental. Indeed, whereas insights for granular boundary flow would render the dataset inapplicable, the saltation threshold can be seen as an upper limit in the case of draping deposits or as a minimum if erosion plays a role and is due to the fluid-phase competence. These considerations taken into account, our dataset can provide valuable information on PDC dynamics.

The results of the influence of slope also provide new insights on the formation of stoss-aggrading structures deposited from dilute PDCs. The gravity-induced difference in the saltation threshold between a (upsloping) stoss side and (downsloping) lee side might indeed explain those structures. It also brings some new perspective on some deposit feature interpretation, and possibly over-estimated flow velocities for parental dilute PDCs.

Further effort will be needed in order to account for the specificities of PDCs. The dynamic saltation threshold and the influence of particle concentration within the flow should be a priority for future experimental designs. Although the measurements presented here represent but a first order approach towards the quantitative interpretation of deposits, this tool can also be powerful to constrain numerical input parameters and global understanding of pyroclastic density currents.

Acknowledgments

Olivier Roche and Pierfrancesco Dellino are acknowledged for valuable reviews. The pumice particles used in this study were kindly offered by ROTEC GmbH & Co. KG (Mühlheim-Kärlich), the scoria particles by Paul Link GmbH & Co. KG (Kretz). We are grateful to the ESA grant TNA2-Europlanet that supported the experiments in Aarhus. GAD and UK are financially supported by the Deutsche Forschungsgemeinschaft grant KU2689/2-1. GAD was partially funded by THESIS Elite Network of Bavaria. DBD acknowledges a Research Professorship (LMUexcellent) of the Bundesexzellenzinitiative and the support of the ERC Advanced Research Grant—EVOKES (No 247076).

References

Allen, J.R.L., 1982. Sedimentary Structures. Their Character and Physical Basis. Elsevier Science Publishers, Amsterdam (663 pages).
Andreotti, B., 2004. A two-species model of aeolian sand transport. J. Fluid Mech. 510, 47–70.
Andrews, B.J., Manga, M., 2012. Experimental study of turbulence, sedimentation, and coignimbrite mass partitioning in dilute pyroclastic density currents. J. Volcanol. Geotherm. Res. 225, 30–44.
Arnott, R.W.C., Hand, B.M., 1989. Bedforms, primary structures and grain fabric in the presence of suspended sediment rain. J. Sed. Res. 59.
Bagnold, R.A., 1941. The Physics of Blown Sand and Desert Dunes. William Morrow and Company, New York.
Bauer, B.O., Houser, C.A., Nickling, W.G., 2004. Analysis of velocity profile measurements from wind-tunnel experiments with saltation. Geomorphology 59, 81–98.
Bonadonna, C., Ernst, G.G.J., Sparks, R.S.J., 1998. Thickness variations and volume estimates of tephra fall deposits: the importance of particle Reynolds number. J. Volcanol. Geotherm. Res. 81, 173–187.
Boudon, G., Lajoie, J., 1989. The 1902 Pelean deposits in the Fort Cemetery of St. Pierre, Martinique: a model for the accumulation of turbulent nuées ardentes. In: Boudon, G., Gourgaud, A. (Eds.), Mount Pelee. J. Volcanol. Geotherm. Res., 38, pp. 113–130.
Bradbury, R., 1953. Fahrenheit 451 Ballantine Books.
Brand, B.D., Clarke, A.B., 2012. An unusually energetic basaltic phreatomagmatic eruption: using deposit characteristics to constrain dilute pyroclastic density current dynamics. J. Volcanol. Geotherm. Res. 243–244, 81–90.
Branney, M.J., Kokelaar, P., 1997. Giant bed from a sustained catastrophic density current flowing over topography: Acatlán ignimbrite, Mexico. Geology 25 (2), 115–118.
Branney, MJ., Kokelaar, P., 2002. Pyroclastic density currents and the sedimentation of ignimbrites. Geological Society Memoir no 27, London.
Brown, R.J., Branney, M.J., 2004. Bypassing and diachronous deposition from density currents: evidence from a giant regressive bed form in the Poris ignimbrite, Tenerife, Canary Islands. Geology 32, 445–448.
Burgisser, A., Bergantz, G.V., 2002. Reconciling pyroclastic flow and surge: the multiphase physics of pyroclastic density currents. Earth Planet. Sci. Lett. 202, 405–418.
Carey, S.N., 1991. Transport and deposition of tephra by pyroclastic flows and surges. Sedimentation in Volcanic Settings SEPM (Special Publication No 45.).
Church, M., Wolcott, J., Maizels, J., 1990. Palaeovelocity: a parsimonious proposal. Earth Surf. Process. Landf. 15, 475–480.
Creyssels, M., Dupont, P., Ould El Moctar, A., Valance, A., Cantat, I., Jenkins, J.T., Pasini, J.M., Rasmussen, K.R., 2009. Saltating particles in a turbulent boundary layer: experiment and theory. J. Fluid Mech. 625, 47–74.
Crowe, B.M., Fisher, R.V., 1973. Sedimentary structures in base-surge deposits with special reference to cross-bedding, Ubehebe Craters, Death Valley, California. Geol. Soc. Am. Bull. 84, 663–682.
Dellino, P., La Volpe, L., 2000. Structures and grain size distribution in surge deposits as a tool for modelling the dynamics of dilute pyroclastic density currents at La Fossa di Vulcano Aeolian Islands, Italy. J. Volcanol. Geotherm. Res. 96, 57–78.
Dellino, P., Isaia, R., La Volpe, L., Orsi, G., 2004a. Interaction between particles transported by fallout and surge in the deposits of the Agnano-Monte Spina eruption (Campi Flegrei, Southern Italy). J. Volcanol. Geotherm. Res. 133, 193–210.
Dellino, P., Isaia, R., Veneruso, M., 2004b. Turbulent boundary layer shear flows as an approximation of base surges at Campi Flegrei (Southern Italy). J. Volcanol. Geotherm. Res. 133, 211–228.
Dellino, P., Mele, D., Bonasia, R., Braia, G., La Volpe, L., Sulpizio, R., 2005. The analysis of the influence of pumice shape on its terminal velocity. Geophys. Res. Lett. 32, L21306.
Dellino, P., Mele, D., Sulpizio, R., La Volpe, L., Braia, G., 2008. A method for the calculation of the impact parameters of dilute pyroclastic density currents based on deposits particle characteristics. J. Geophys. Res. 113, B07206.
Doronzo, D.M., Dellino, P., 2011. Interaction between pyroclastic density currents and buildings: numerical simulation and first experiments. Earth Planet. Sci. Lett. 310, 286–292.
Douillet, G.A., Tsang-Hin-Sun, E., Kueppers, U., Letort, J., Pacheco, D.A., Lavallee, Y., Goldstein, F., Hanson, J.B., Bustillos, J., Robin, C., Ramón, P., Dingwell, D.B., 2013a. Cross-stratified, ash sedimentary wedges deposited from the 2006 dilute pyroclastic density currents at Tungurahua volcano, Ecuador. Bull. Volcanol. 75, 765.
Douillet, G.A., Pacheco, D.A., Kueppers, U., Tsang-Hin-Sun, E., Dingwell, D.B., 2013b. Dune bedforms produced by the 2006 pyroclastic density currents at Tungurahua volcano, Ecuador. Bull. Volcanol. 75, 762.
Druitt, T.H., 1996. Pyroclastic density currents. In: Gilbert, J.S., Sparks, R.S.J. (Eds.), The Physics of Explosive Volcanic Eruptions. Geological Society, London, Special Publications, 145, pp. 145–182.
Durán, O., Hermann, H., 2006. Modeling of saturated sand flux. J. Stat. Mech. 7, P07011.
Durán, O., Claudin, P., Andreotti, B., 2011. On aeolian transport: grain-scale interactions, dynamical mechanisms and scaling laws. Aeolian Res. 3, 243–270.
Fisher, R.V., Waters, A.C., 1969. Bed forms in base surge deposits: lunar implications. Science 165, 1349–1352.
Garratt, J.R., 1992. The Atmospheric Boundary Layer. Cambridge Atmospheric and Space Science Series.
Grimmond, C.S.B., Oke, T.R., 1998. Aerodynamic properties of urban areas derived from analysis of surface form. J. Appl. Meteorol. 38, 1262–1292.
Iversen, J.D., Rasmussen, K.R., 1994. The effect of surface slope on saltation threshold. Sedimentology 41, 721–728.
Iversen, J.D., Rasmussen, K.R., 1999. The effect of wind speed and bed slope on sand transport. Sedimentology 46, 723–731.
Iversen, J.D., Pollack, J.B., Greeley, R., White, B.R., 1976. Saltation threshold on Mars: the effect of interparticle force, surface roughness, and low atmospheric density. Icarus 29, 381–393.
Iversen, J.D., Greeley, R., Marshall, J.R., Pollack, J.B., 1987. Aeolian saltation threshold: the effect of density ratio. Sedimentology 34, 699–706.
Kieffer, S.W., Sturtevant, B., 1988. Erosional furrows formed during the lateral blast at Mount St. Helens, May 18, 1980. J. Volcanol. Geotherm. Res. 93 (B12), 14793–14816.
Kok, J.F., Renno, N.O., 2009. A comprehensive model of steady state saltation (COMSALT). J. Geophys. Res. 114, D17204.
Lacroix, A., 1904. La Montagne Pelée et ses éruptions. Masson, Paris.
Lajoie, J., Boudon, G., Bourdier, J.L., 1989. Depositional mechanics of the 1902 pyroclastic nuée ardente deposits of Mt. Pelée, Martinique. J. Volcanol. Geotherm. Res. 38, 131–142.

Lang, J., Winsemann, J., 2013. Lateral and vertical relationships of bedforms deposited by aggrading supercritical flows: from cyclic steps to humpback dunes. Sediment. Geol. 296, 36–54. http://dx.doi.org/10.1016/j.sedgeo.2013.08.005.
Le Roux, J.P., 2005. Comments on "Turbulent boundary layer shear flows as an approximation of base surges at Campi Flegrei (Southern Italy), by Dellino et al. (2004). J. Volcanol. Geotherm. Res. 141, 331–332.
Lullin, A., 1925. Recherches sur les températures d'inflammation du bois et sur les enduits ignifuges. PhD Thesis Ecole Polytechnique fédérale Zurich.
Merrison, J.P., 2012. Sand transport, erosion and granular electrification. Aeolian Res. 4, 1–16.
Middleton, G.V., 1976. Hydraulic interpretation of sand size distributions. J. Geol. 84, 405–426.
Miller, M.C., McCave, I.N., Komar, P.D., 1977. Threshold of sediment motion under unidirectional currents. Sedimentology 24, 507–527.
Nikuradse, J., 1933. Stromungsgesetze in rauhen Rohren: VDI Forschungsheft 361. translation by National Advisory Committee on Aeronautics, Technical Memorandum No. 1292, Washington, DC, 1950.
Owen, P.R., 1964. Saltation of uniform grains in air. J. Fluid Mech. 20 (2), 225–242.
Prave, A.R., 1990. Clarification of some misconceptions about antidunes geometry and flow character. Sedimentology 37, 1049–1052.
Rasmussen, K.R., Mikkelsen, H.E., 1990. Wind Tunnel observations of aeolian transport rates. Acta Mech. 1 (Suppl. 2), 135–144.
Rasmussen, K.R., Iversen, J.D., Rautaheimo, P., 1996. Saltation and wind–flow interaction in a variable slope wind tunnel. Geomorphology 17, 19–28.
Sherman, D.J., 1992. An equilibrium relationship for shear velocity and apparent roughness length in aeolian saltation. Geomorphology 5, 419–431.
Shields, A., 1936. Application of similarity principles and turbulence research to bed-load movement. Mitteilungen der Preussischen Versuchsanstalt fur Wasserbau und Schifbau, Berlin. In: Ott, W.P., van Uchelen, J.C. (Eds.), California Inst. Tech., W.M. Keck Lab. of Hydraulics and Water Resources, Rept. No. 167.
Simons, D.B., Richardson, E.V., Haushild, W.L., 1963. Some effects of fine sediment on flow phenomena. U. S. Geol. Surv. Water Supply Pap. 1498-G (47 pp.).
Sohn, Y.K., 1997. On traction carpet sedimentation. J. Sed. Res. 67 (3), 502–509.
Sparks, R.S.J., 1976. Grain size variations in ignimbrites and implications for the transport of pyroclastic flows. Sedimentology 23, 147–188.
Sparks, R.S.J., 1983. Mont Pelée Martinique May 8 and May 20 1902 pyroclastic flows and surges—discussion. J. Volcanol. Geotherm. Res. 19, 175–184.
Sparks, R.S.J., Wilson, L., Hulme, G., 1978. Theoretical modeling of the generation, movement and emplacement of pyroclastic flows by column collapse. J. Geophys. Res. 83, 1727–1739.
Sulpizio, R., Mele, D., Dellino, P., La Volpe, L., 2007. Deposits and physical properties of pyroclastic density currents during complex Subplinian eruptions: the AD 472 (Pollena) eruption of Somma-Vesuvius, Italy. Sedimentology 54, 607–635.
Sulpizio, R., Bonasia, R., Dellino, P., Mele, D., Di Vito, M.A., La Volpe, L., 2010. The pomici di avellino eruption of Somma-Vesuvius (3.9 ka BP). Part II: sedimentology and physical volcanology of pyroclastic density current deposits. Bull. Volcanol. 72 (5), 559–577.
Sumner, E.J., Amy, L.A., Talling, P.J., 2008. Deposit structure and processes of sand deposition from decelerating sediment suspensions. J. Sed. Res. 78, 529–547.
Tanguy, J.C., Ribière, C., Scarth, A., Tjetjep, W.S., 1998. Victims from volcanic eruptions: a revised database. Bull. Volcanol. 60, 137–144.
Valentine, G.A., 1987. Stratified flow in pyroclastic surges. Bull. Volcanol. 49, 616–630.
Vallis, G.K., 2006. Atmospheric and Oceanic Fluid Dynamics—Fundamentals and Large Scale Circulation. Cambridge University Press (ISBN: 978-0-521-84969-2).
Walker, G.P.L., 1971. Grain-size characteristics of pyroclastic deposits. J. Geophys. Res. 79, 619–714.
Walker, G.P.L., 1984. Characteristics of dune-bedded pyroclastic surge bedsets. J. Volcanol. Geotherm. Res. 20, 281–296.
Walker, G.P.L., McBroome, L.A., 1983. Mount St. Helens 1980 and Mount Pelée 1902—flow or surge. Geology 11, 571–574.
Walker, G.P.L., Wilson, L., Bowell, E.L.G., 1971. Explosive volcanic eruptions—I. The rate of fall of pyroclasts. Geophys. J. R. Astron. Soc. 22, 377–383.
Wohletz, K.H., 1998. Pyroclastic surges and compressible two-phase flow. In: Freundt, A., Rosi, M. (Eds.), From Magma to Tephra. Elsevier, Amsterdam, p. 25.
Zheng, X., He, L., Wu, J., 2004. Vertical profiles of mass flux for windblown sand movement at steady state. J. Geophys. Res. 109, B01106. http://dx.doi.org/10.1029/2003JB002656.